IAC-09-A3.4.10

"THE EXTREME ULTRAVIOLET IMAGER (EUI) ONBOARD THE SOLAR ORBITER MISSION"

P. Rochus [(1)], J.-P. Halain[(1)], E. Renotte[(1)], D. Berghmans[(2)], A. Zhukov [(2)], J-F. Hochedez [(2)], T. Appourchaux[(3)], F. Auchère[(2)], L. K. Harra[(4)], U. Schühle[(5)], R.Mercier[(6)]

and the EUI consortium

[(1)] *Centre Spatial de Liège, Belgium* , prochus@ulg.ac.be
[(2)] *Royal Observatory of Belgium, Belgium, j-f.hochedez@sidc.be*
[(3)] *Institut d'Astrophysique Spatiale, France, thierry.appourchaux@ias.u-psud.fr*
[(4)] *Mullard Space Science Laboratory, United Kingdom, lkh@mssl.ucl.ac.uk*
[(5)] *Max-Planck-Institut für Sonnensystemforschung, Germany, schuehle@mps.mpg.de*
[(6)] *Institut d'Optique, France*

ABSTRACT

Solar Orbiter will for the first time study the Sun with a full suite of in-situ and remote sensing instruments from inside 0.25 AU and will provide imaging and spectral observations of the Sun's polar regions, from out of the ecliptic. This proximity to the Sun will also have the significant advantage that the spacecraft will fly in near synchronization with the Sun's rotation, allowing observations of the solar surface and heliosphere to be studied from a near co-rotating vantage point for almost a complete solar rotation. The mission's ambitious characteristics draw severe constraints on the design of these instruments. The scientific objectives of Solar Orbiter rely ubiquitously on the Extreme EUV Imager suite (EUI). The EUI instrument suite on board of Solar Orbiter is composed of two high resolution imagers (HRI), one at Lyman α and one dual band at the two 174 and 335 EUV passbands in the extreme UV, and one dual band full-sun imager (FSI) working alternatively at the two 174 and 304 EUV passbands. In all the units, the image is produced by a mirror-telescope, working in nearly normal incidence. The EUV reflectivity of the optical surfaces is obtained with specific EUV multilayered coatings, providing the spectral selection of the EUV units (1HRI and 1 FSI). The spectral selection is complemented with very thin filters rejecting the visible and IR radiation. Due to its orbit, EUI / Solar Orbiter will see 20 solar constants and an entrance baffle to limit the solar heat input into EUI is needed. The paper presents the scientific objectives of EUI and also covers the EUI instrument development plan which will require some trade-off between existing and promising technologies.

1. INTRODUCTION

The Solar Orbiter mission, a candidate mission in the ESA Cosmic Vision Science Programme, is devoted to the Sun and the new discipline of heliophysics, which arose from ESA's successful SOHO mission launched in 1995. From its unique vantage point in an elliptical orbit around the Sun, and approaching as close as 48 solar radii, Solar Orbiter will provide unprecedented close-up and high-latitude observations of the Sun. Solar Orbiter will be carried out as an ESA-led mission open to the worldwide science community. The Extreme Ultraviolet Imager (EUI) instrument was selected by ESA as part of the scientific payload for the ESA Solar Orbiter mission. The instrument and the scientific rationale summarized in this paper have been studied by scientists and engineers from the Centre Spatial de Liège, the Royal Observatory of Belgium, the Institut d'Astrophysique Spatiale, the Max Planck Institute for Solar System Research and the Mullard Space Science Laboratory. The payload complement will support scientific investigations ranging from near-Sun and out-of-ecliptic in-situ measurements to remote-sensing observations of the Sun and its environs.

In the mean time, NASA decided to implement the Solar Probe Plus (SPP) mission in the same time-frame as Solar Orbiter. Solar Orbiter Payload Re-evaluation Panel was convened to conclude that the selected payload is still valid in the context of a joint program with SPP.

The scientific objectives of Solar Orbiter rely ubiquitously on EUI. The EUI instrument suite on board of Solar Orbiter is composed of two high resolution imagers (HRI), one at Lyman α and one dual band in the extreme UV, and one dual band full-sun imager (FSI) working alternatively at the two 174 and 304 EUV passbands.

The instrumental scientific objectives are described in the next section. Section 3 details the scientific requirements on the EUI suite. EUI technical layout is presented in section 4. Section 5 highlights some of the foreseen challenges that the EUI development will face. Conclusions can be found in Section 6.

2. EUI SCIENTIFIC OBJECTIVES

The exceptional orbits of the Solar Orbiter mission will allow us to achieve breakthroughs in plasma astrophysics by imaging the magnetized solar atmosphere in the extreme-ultraviolet (EUV) emission. In comparison with current EUV imagers (EIT, TRACE, SECCHI/EUVI and AIA/SDO), a major advance is to obtain very high resolution images (160 km, i.e. 5 times better than TRACE) due to the position of the orbit perihelion close to the Sun. Another major breakthrough will be achieved by taking first ever images of the Sun from an out-of-ecliptic viewpoint (up to 34° of solar latitude during the extended mission phase (Figure 1).

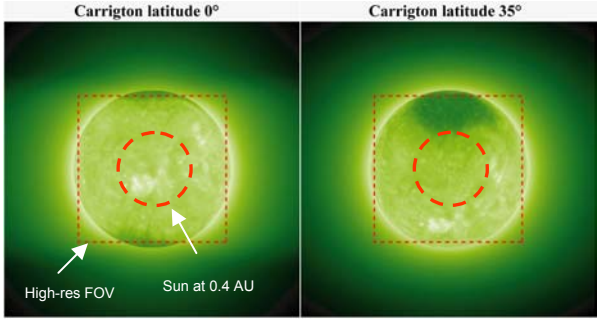

Figure 1: Simulations of the Sun as seen by FSI from two heliographic latitudes : 0 ◦(left) and 35◦(right). The size of the Sun corresponds to the perihelion of Solar Orbiter (0.2 AU). The dashed squares represent the inner 2048 × 2048 pixels subfield that can be transmitted at the maximum resolution of 4.5"/pixel.Field of View at 0.2 AU

The scientific objectives of Solar Orbiter rely ubiquitously on the Extreme-Ultraviolet Imager (EUI), a suite of imaging telescopes to observe the solar atmosphere. EUI will allow us, on one hand, to provide a crucial understanding of fine scale processes in the highly structured and dynamic solar atmosphere and, on the other hand, to determine the global structure of the solar corona. Images taken by the Full Sun Imager (FSI) of the EUI suite will offer the indispensable link between the solar surface and the outer corona, which ultimately shapes the characteristics of the interplanetary medium to be sampled in situ by Solar Orbiter and Solar Probe+. The two High Resolution Imagers (HRIs) will provide nearly simultaneous view of the solar atmosphere in three complementary band passes. They will image the upper chromosphere, the quiescent and the active corona –including coronal holes-, thus providing a comprehensive view of the solar atmosphere dynamics under different conditions. Due to its large field of view, EUI/FSI is the only instrument able to provide the images of the full-disc corona and thus can play a central role in coordination of observations of the solar atmosphere by the remote-sensing instruments onboard Solar Orbiter. EUI will also observe the onset of eruptive solar phenomena such as solar flares and coronal mass ejections (CMEs) that can possibly lead to powerful solar energetic particle events.

Science objectives	EUI observations
What are the origins of the solar wind streams and the heliospheric magnetic field? *(HELEX JSTDT report 2.1)*	Large scale coronal structure, coronal hole boundaries, chromospheric network, plumes, spicules, funnels, active regions, base of streamers
What are the sources, acceleration mechanisms, and transport processes of solar energetic particles? *(HELEX JSTDT report 2.2)*	Identification of flare and CME sites and their evolution, overall active region magnetic topology, post-eruption arcades, flare ribbons, EIT waves, jets
How do coronal mass ejections evolve in the inner heliosphere? *(HELEX JSTDT report 2.3)*	CME onset detection and CME source region evolution, filaments, prominences, dimmings, EIT waves
Explore, at all latitudes, the energetic, dynamic and fine-scale structure of the Sun's magnetized atmosphere. *(Solar Orbiter Sci-RD 2.3)*	Loops, plumes, jets, moss, waves, super granular cells, spicules, funnels, active regions

Table 1 : Scientific objectives and EUI observations

The overall structure of the heliosphere and the related solar global boundary conditions are reasonably well understood from space missions such as Helios, Ulysses and SOHO, with fast solar wind streams linked to magnetically open coronal holes and slow solar wind originating in the dense streamer belt in the solar corona. However, this global description does not address the detailed solar origin of individual solar wind streams. The connections of many solar phenomena with their manifestations in the heliosphere are still not clear. EUI will provide unique images of solar polar coronal holes taken from a high-latitude vantage point and image the regions of the nascent solar wind in the solar transition region and corona with unprecedented detail.

The most prominent features within polar coronal holes (sources of fast solar wind streams) are plumes – bright ray-like structures that extend over several solar radii. Plumes are cooler and denser than the surrounding corona and will be well observed by the HRI. Whether the fast solar wind streams originate

also from plumes or mostly inter-plume regions is still a matter of debate. This controversy is difficult to settle because of the location of the present-day remote sensing platforms, all near the ecliptic plane, creating ambiguities due to the integration along a line of sight which includes non-hole plasma. It is also essential to establish whether there is a link between the plumes observed in the corona and the narrow density structures detected in situ in the fast solar wind. It can be expected that near the Solar Orbiter and Solar Probe+ perihelia (around 48 and 9.5 solar radii respectively) the fast solar wind will not be as uniform as observed by Ulysses at greater distances. The out-of-ecliptic and the close-up viewpoints of Solar Orbiter will help to resolve those problems and allow us to study plumes and polar jets with unprecedented details in all HRI channels. This will provide crucial insight in the elusive acceleration mechanism of the solar wind.

Recent research has confirmed the association of the fast solar wind with coronal funnels, expanding magnetic field structures rooted in the magnetic network lanes. Their possible link with kilogauss magnetic fields in polar faculae is still uncertain. The solar wind starts flowing out of the corona in these funnels at heights beyond 5 Mm above the photosphere. HRI and SPICE together with PHI will be able to observe this process at smaller scales than previously possible. FSI images will be combined with the METIS/COR white light images of the inner corona (using the overlap of the two fields of view) to map and follow the evolution of coronal holes and their fine structures. The same is true for closed field structures such as streamers.

EUI will gain an important and detailed understanding of fundamental processes of energy release in the magnetized solar corona operating at fine spatial and temporal scales, so far inaccessible to current space- and ground-based solar instrumentation. The solar atmosphere appears extremely structured and dynamic when observed at the best present spatial resolution: about 700 km in the corona (TRACE), 250 km in the transition region (VAULT), about 100 km in the photosphere and chromosphere (Hinode/SOT and ground-based telescopes). Small filling factors in the coronal plasma recently measured on the base of the Hinode/EIS data also indicate unresolved structuring. Plasma of very different temperatures (104 – 107 K) may co-exist side by side in hierarchies of loops of different dimensions channeled by the magnetic field, together forming the solar atmosphere. The smallest-scale structures appear at the limit of instruments' spatial resolution. Therefore, it is possible that elementary structures are not yet resolved Figure 2.

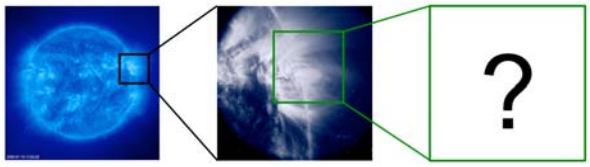

Figure 2. The field of view of the HRI telescope of the EUI suite onboard Solar Orbiter (right) as compared with SOHO/EIT (left) and TRACE (middle) images showing coronal loops, the building blocks of the solar atmosphere. Pixel size on the Sun of EIT and TRACE is 1850 and 350 km respectively. EUI onboard Solar Orbiter will have a pixel size of 80 km on the Sun.

The spatio-temporal structuring of plasma and magnetic fields in the solar atmosphere determines the dominant fundamental physical processes (from MHD to kinetic) of energy dissipation that lead to plasma heating, cooling, radiation, motion and wave generation, as well as solar wind and energetic particle acceleration. These fundamental processes, in turn, influence the fine structure of the corona. The dominant space and time scales of energy storage and dissipation still remain elusive. The HRI, with its 160 km spatial resolution (i.e. 80 km pixel size at the perihelion) will allow significant progress to be made in the study of the fine structure and dynamical processes in the solar transition region (TR) and corona. The Sun is the only star that can be resolved down to the level at which the physical processes responsible for magnetic activity take place.

Yohkoh/SXT, EIT and TRACE images indicate that coronal loops do not expand systematically with height. They have instead a uniform cross section, contrary to the geometry of magnetic flux tubes that can be derived from extrapolations of photospheric magnetograms. It was suggested that loops with uniform width might be compatible with a complex internal loop structure of tangled elementary flux tubes with non-uniform geometry. We expect that the HRI will be able to resolve the elementary loops (strands) and other fine scale structures and thus to clarify this issue. In addition, the heating of the solar atmosphere and its small-scale structuring (jets, spicules, macrospicules and the newly discovered straws from Hinode/SOT) seem to be intimately linked with the formation of the solar wind, and hence understanding the small-scale structure will be crucial for the solar wind acceleration studies.

The interaction between the lower atmosphere and the corona continues to be a mystery. SOHO/SUMER and Lyman-α observations by VAULT reveal that, in the quiet Sun, the lower to mid TR is formed by many loop-like structures located along and across network

boundaries (and also in the network cell centres), with widths at or below the instrument spatial resolution (1400 km for SUMER, 250 km for VAULT). These observations seem to support the unresolved fine structure concept of the TR suggesting that the corona is magnetically disconnected from most of the transition region. However, it is not clear whether these loop-like structures are footpoints of coronal loops or separate independent cool loops. Nearly simultaneous images at high spatio-temporal resolution in three HRI channels will help us to test different scenarios of the connection between the corona and the transition region.

3. SCIENTIFIC REQUIREMENTS ON EUV IMAGING

3.1 Requirements for full Sun imaging

Full Sun EUV imaging should provide images of the cold and hot layers of the solar atmosphere along the whole mission orbit. The quiescent, large-scale corona can be imaged in the spectral bandpass centred at 174 Å and dominated by Fe IX/X emission lines formed at temperatures around 0.8–1.1 MK. The lower transition region can be imaged in the 304 Å bandpass dominated by the He II emission line formed at a temperature around 0.08 MK (or lower). Simultaneity of images in two bandpasses is not required. Both bandpasses can thus be combined inside a single telescope. The telescope aperture of 0.5 cm allows achieving acceptable signal-to-noise ratios with exposure times between 1 s and 10 s allowing a cadence of around 10 minutes in each bandpass (to allow the observations of solar eruptive events such as CMEs and flares). The field of view should be large enough to image the full Sun even if the spacecraft performs off-point observations centred on the solar limb near the perihelion of the orbit, namely 5.2 degrees. The spatial resolution should be 760 km at the perihelion (0.22 AU) and 2900 km at the aphelion (0.86 AU) with a detector of 4096x4096 pixels.

3.2 Requirements for high-resolution imaging

High-resolution EUV imaging should provide images of the chromosphere, quiescent corona and active corona. Three suitable bandpasses are: H I Lyman-α at 1216 Å (emission of the upper solar chromosphere formed at temperatures around 0.02 MK), Fe IX/X at 174 Å (emission of the quiescent corona formed at temperatures around 0.8–1.1 MK) and Fe XVI at 335 Å (emission of the active corona formed at 2.6 MK). The last two bandpasses will be combined in the single telescope to save mass. The operational periods for high-resolution imagers include encounter phases (30 days centred at the orbit perihelion), periods of highest northern and southern solar latitudes and special configurations with the Solar Probe+ mission (quadratures and conjunctions). During the rest of the orbit high-resolution imagers are not operational.

Due to the strength of the H I Lyman-α line, it is possible to reach a very high cadence (sub-second) in this bandpass to observe dynamic phenomena in the supergranulation network at the source of the solar wind and in active regions. The observations in the Lyman-α bandpass should be simultaneous with a coronal bandpass. Apertures of 30 mm will allow reaching the observational cadence of 2 seconds in the 174 Å coronal bandpass. The effective spatial resolution of high-resolution imagers at perihelion is required to be 1 arc sec (i.e. 160 km). The corresponding field of view is 0.24 solar radii (with detectors of 2048x2048 pixels). The improvement of factor 5 in spatial resolution in comparison with TRACE is matched by a similar improvement in the cadence (factor 6), thus maintaining a combination of the cadence and spatial resolution necessary for observation of small-scale events in the solar atmosphere.

4. INSTRUMENTAL CONFIGURATION

4.1 Functional description

4.1.1 Measurement principle

The EUI instrument suite is composed of two high resolution imagers (HRI), one at Lyman-α and one dual band in the extreme UV alternatively at 174 and 335Å, respectively named "$HRI_{Ly\text{-}\alpha}$" and "HRI_{EUV}", and one dual band full-sun imager (FSI) working alternatively at the 174 and 304 Å EUV passbands, named "$FSI_{174/304}$".

In all the units, the image is produced by a mirror-telescope, working in nearly normal incidence. The EUV reflectivity of the optical surfaces is obtained with specific EUV multilayered coatings. The spectral selection is complemented with bandpass filters rejecting the visible and IR radiation. The UV photons reach detectors (back-thinned APS detectors of 2k x 2k format for the HRI channels and 4k x 4k format for the FSI channel) where they are converted into electrical charges that are amplified into volts, and digitized by an A/D converter. For each detector pixel, the resulting signal in DN is proportional to the exposure time and to the solar flux corresponding to the small viewing angle of the pixel in the given band pass.

Figure 3 shows the functional diagram of the HRI and FSI telescopes, including the front filter and its protection mechanism (door) and entrance baffle, the EUV filters wheels mechanisms and telescope (i.e. mirrors), the detector and proximity electronic acquisition chain, and the common electronic.

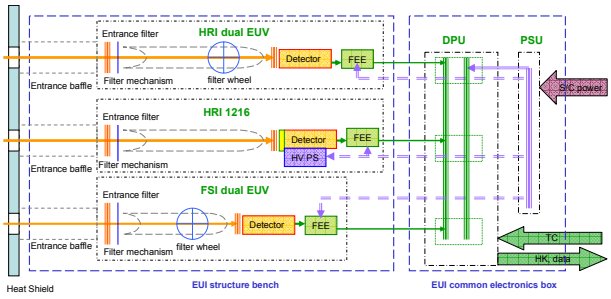

Figure 3: FSI and HRIs Functional diagram.

4.1.2 Hardware description

4.1.2.1 Overall design

4.1.2.1.1 Mechanical configuration

The proposed baseline mechanical configuration is shown on *Figure 4*, with the three channels on one side of a common optical bench with dedicated isostatic mounts, and a common electronics box (CEB) as a separate unit. This concept has been optimized for mechanical and thermal constraints. One additional advantage of two separated units (bench and CEB) is to allow parallel optical and electrical developments and sub-systems testing.

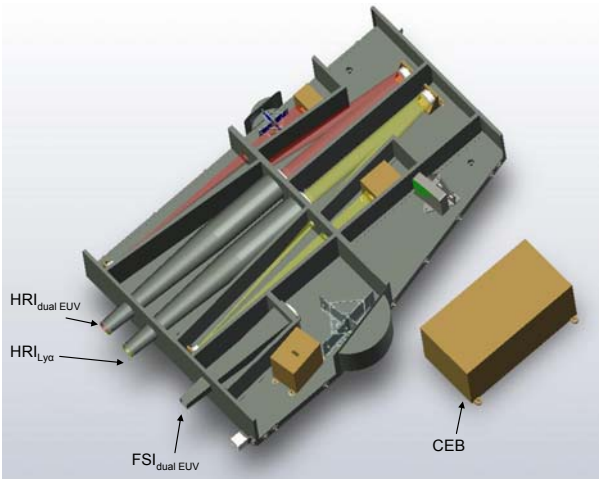

Figure 4 : Overall of the EUI baseline instrument

The three channels share a common optical bench structure made out of a CFRP sandwich panel with an aluminum honeycomb core to meet stiffness and thermal stability requirements while achieving a low mass. The mounting points are made out of titanium inserts, bonded into the panel. Per unit, three mounting points will be available including locators (dowel pins or flats) in order to be able to maintain alignment when units are taken off and put back on again. Each optical sub-system, either primary mirror or secondary mirror, filter wheel or Focal Plane Assembly (FPA) will have their separate interface. This arrangement allows for clearly defined interfaces with an absolute minimum in thermal-elastic deformation for each instrument, and in particular mirrors inter-distance and channel co-alignment stability. A cover will provide for additional stiffness if needed to add torsional and bending stiffness to the overall structure. The mounts will minimize the thermal and mechanical couplings between EUI and the platform, and provide sufficient stiffness to guarantee a sufficiently high first eigenfrequency. Table 2 specifies the intended temporal and spatial resolutions, field-of-view (FOV) as well as passbands.

Channel	Parameter	Values
	Dimensions • Optical bench • CEB	 • 900x600x230mm • 120x300x250mm
	Mass (including margins)	18.20kg
	Nominal power consumption	32 W
	Telemetry	20.5 kb/s
FSI dual EUV	Passband centre	174 Å and 304 Å alternatively
	Field of View	5.2 arcdeg × 5.2 arcdeg
	Angular resolution (2 px)	9 arcsec
	Typical cadence	600 s
HRI dual EUV	Passband centre	174 Å and 335 Å alternatively
	Field of View	1000 arc sec square
	Angular resolution (2 px)	1 arcsec
	Typical high cadence	2 s
HRI Lyman-α	Passband centre	1216 Å
	Field of View	1000 arcsec square
	Angular resolution (2 px)	1 arcsec
	Typical high cadence	Sub-second

Table 2: Main characteristics of the EUI channels

The technology for building the EUI instrument under the challenging constraints of the Solar Orbiter mission is at a high level of maturity and builds on heritage from past missions. Pre-launch and in-flight calibrations will be implemented to assure that the EUI data are suitable for quantitative scientific analysis.

4.1.2.2 Channels description

The two HRI units share a quasi-identical optical design. It is based on an off-axis Gregory telescope optimized in length with a 30 mm diameter entrance pupil located at the front section of the entrance baffle, to guarantee a sufficient overall instrument throughput. This entrance baffle is designed to provide a first level of protection against straylight from the overall solar disk, and also a reduction of the heat input reaching the entrance foil filter. The above-stated aperture diameter is compliant with the heat input specifications. The FSI unit is based on an Herschelian telescope optimized with a 5mm diameter aperture pupil.

The optical design parameters of the EUI channels are detailed hereafter. Tolerance analyses have been performed to evaluate the capability of the concept to maintain good image quality with an opto-mechanical structure submitted to the varying thermal conditions associated to the Science Operation Windows. The resulting requirements for the thermo-mechanical environment indicate that a CFRP composite structure combined with fused silica mirrors (TBC) and Invar mounts is required to keep performances within the expected thermal excursions.

4.1.2.2.1 HRI_{EUV} channel

The dual-band HRI_{EUV} channel (Figure 5) is an off-axis Gregory telescope.

One aluminum foil filter is inserted between the entrance aperture (entrance pupil) and the primary mirror to provide protection against excessive heat input on the mirror and efficient rejection of the visible light. A filter wheel is located at the output pupil for wavelength selection. These EUV filters are of primary importance for the instrument in order to avoid contamination with visible light that can be 10^8 times more intense than the EUV flux.

The EUV reflective coatings of the mirrors are specific multilayers optimized to provide the optimal spectral passbands. Their design takes into account the angle of incidence on the mirrors, the variations of which are small enough so that no compensation is needed. The HRI_{EUV} unit uses a 2k x 2k APS detector. The APS solution provides rolling or global electronic shutter operation capability, and avoids the need for a mechanical shutter.

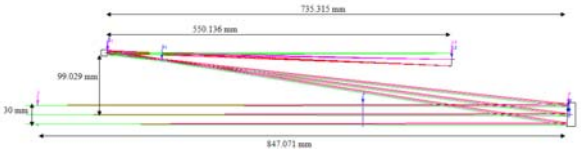

Figure 5: HRI_{EUV} channel optical design.

	HRI_{EUV}	$HRI_{Ly-\alpha}$
Focal length	4122.879 mm	6000 mm
Entrance pupil	ϕ 30 mm	ϕ 30 mm
Field of view	1000 arcsec square	1000 arcsec square
Plate scale	50 arcsec/mm	31.5 arcsec /mm (after intensifier reductor)
Detector	2048 x 2048, 10 µm	2048 x 2048, 10 µm
M1-M2 distance	735 mm	735 mm
M2 – detector distance	550.136 mm	600 mm
Primary mirror	ϕ 35.4 mm parabolic radius -1303.471 mm off-axis distance 87.38 mm	ϕ 36 mm parabolic radius 1293.0 mm off-axis distance 100 mm
Secondary mirror	ϕ 8.6 mm hyperbolic radius 150.17 mm off-axis distance 11.576 mm	ϕ 10 mm hyperbolic radius -104.4 mm off-axis distance 7.30 mm

Table 3: Design parameters of the HRI_{EUV} and HRI_{Ly-a} channels

4.1.2.2.2 $HRI_{Ly-\alpha}$ channel

The Lyman-α HRI channel uses a design very similar to that of the EUV filtergraph. It is likewise a Gregory off-axis system as illustrated in Figure 6. The optical design parameters are detailed in Table 3. The main difference of the Lyman-α channel lies in the mirrors coatings, the EUV foil filter substituted for a specific Lyman-α interference filter and in the detector. The baseline aperture of 30 mm will limit the contrast at the pixel scale due to diffraction but it still provides the required image scale specification of 1-arcsec per 2 pixels.

The Lyman-α channel mirrors use proven technology for the coatings of the primary and secondary mirrors. The Al/MgF2 (aluminum / magnesium fluoride) coating provides reflectivity at 1216 Å over 75%. This optical design provides a high throughput by using a narrow-band and a broadband interference filter on MgF2 substrate to isolate the spectral line at 1216 Å (that is moreover the brightest UV line of the solar emission spectrum). A broad-band interference filter is used at the entrance of the telescope to reject visible and infrared light as well as EUV and X-rays, protecting the mirror coatings. A narrow-band filter will be placed in front of the detector to further isolate the Lyman-α line and achieve the spectral purity. The combination yields a spectral purity of 87% for Lyman-α in the quiet Sun and higher purity in the active regions, and is tolerant to spectral shifts potentially due to thermal effects. The magnesium fluoride substrate is sufficiently radiation hard so as to provide the thermal heat load protection with minimal degradation during the mission.

The detector of the Lyman-α channel will be a solar-blind, intensified 2k x 2k CMOS active pixel sensor (I-APS) with a sensitive aperture of 32x32 mm. The image size of the intensifier is reduced by a fibre optic

taper to the actual size of the CMOS/APS sensor providing a 1 arcsec image on two pixels.

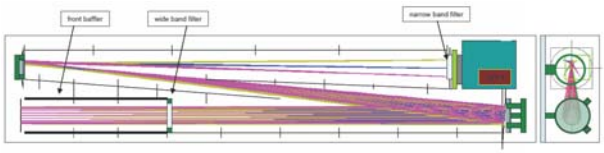

Figure 6: HRI$_{Ly\text{-}\alpha}$ channel detail.

4.1.2.2.3 FSI channel

The FSI optical design is based upon a single off-axis mirror (Herschelian telescope) making an image of a 5.2 deg x 5.2 deg FOV through a 5-mm entrance pupil located at 700 mm from the mirror (equivalent focal length is 450 mm).

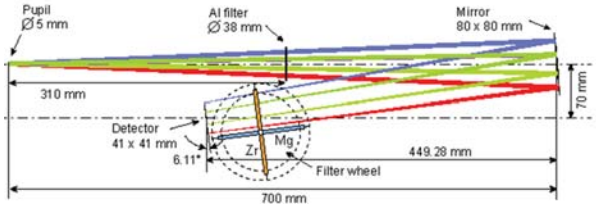

Figure 7: Optical scheme of FSI (TBC).

The optical prescription is given in *Table 4*. A thin film aluminum filter is positioned 310 mm behind the entrance pupil. This filter rejects the white light and the IR in the front baffle, letting only the EUV through. The 174 Å and 304 Å FSI wavebands are selected using thin (zirconium) and an Al/Mg/Al (aluminium/magnesium/aluminium) filters mounted on a filter wheel (*Figure 7*). The flux dilution is such that the flux density at the filter is only 1.3 solar constants at perihelion.

Because the pupil is small compared to the detector, the beam illuminates a 68 x 68 mm² on the mirror. Making the mirror square (80 x 80 mm² with margin) represents 35% mass reduction compared to the equivalent circular mirror (113 mm diameter). Additional mass reduction is achieved (about 50%) by making the back side hollow. The incidence angles on the mirror vary only between 88.8° and 86.3°. This small variation is very favorable for the uniformity of the spectral response of the multilayer coating across the mirror.

The detector is a 4k x 4k 10 µm pitch array. The 174 and 304 Å wavebands are selected using respectively a Zr and an Al/Mg/Al filters respectively mounted on a filter-wheel. Flight-grade filters of these materials are available commercially from several companies. As thin films metallic filters are fragile and can develop pinholes during their lifetime, the filter wheel holds two filters of each kind for redundancy. The filter wheel is a critical component and will be qualified for 1 million operations, which is equivalent to 10 years of operations at 5 minutes cadence.

Optical element	Parameters
Entrance pupil	Shape: circular - Dimensions: Ø 5 mm
Distance Pupil – M1	700 mm
Mirror M1	Figure: off-axis ellipsoid, conic = -0.59 Shape: square 80 × 80 mm Off-axis: 70 mm - Focal length: 450 mm
Distance M1 – Focal plane	449.28 mm
Detector	Figure: flat square 40.96 × 40.96 mm Pixels: 4096 × 4096 Tilt to optical axis : 6.11°

Table 4: Design parameters of the FSI

HRI and FSI have spatial resolutions of 1 arcsec and 9 arcsec respectively. The temporal cadence of HRI depends on the target and can reach sub-second values to observe the fast dynamics of small-scale features. FSI cadence will typically be of the order of 10 minutes in each passband, but it can occasionally reach 10 s. Due to its high-cadence imaging, EUI is capable of producing amounts of data that are incompatible with the limited telemetry allocated to EUI. Two solutions will be implemented. First, state-of-the-art compression algorithms will be developed. A compression factor (10 to 50 will be carefully selected for each EUI passband so as to ensure that the targeted features are not compromised by the compression algorithm. Second, fully autonomous onboard software will be created to perform an intelligent selection of the most interesting data (e.g. observations of an eruptive event) for the transmission to the ground.

The diameter of entrance apertures of HRI telescopes is 30 mm. A special heat rejection baffle for each HRI passband has been designed to limit the heat flux entering the spacecraft.

FSI and one HRI observe in extreme UV passbands, dominated by coronal emission. Another HRI is designed to select the H I Lyman α radiation in the far UV, imaging the Chromosphere and the lower Transition Region (TR) [1].

The FSI FOV amounts to 5.2°, i.e. 4 solar radii at perihelion (0.2 AU) while the HRI pixel corresponds to 160 km at disc centre. The 4k x 4k FSI detector format is worth a comment. Despite the technological challenge that it might represent, it is considered essential in order to bridge the global view uniquely offered by the FSI with the high-resolution payload, including the HRIs. One FSI pixel corresponds here to

					Signal (ph/px/s)			
Channel	Bandpass centre (Å)	FOV (arcmin)	Image scale (arcsec)	Typical cadence rates (s)	CH	QS	AR	Flare ($\times 10^3$)
HRI[a]	174[b]	16.6	0.5	1-100	1.8	9.2	86	0.3 (C1)
	335[b]	16.6	0.5	1-100	0.7	4.5	115	0.7 (C1)
	1216[c,d]	16.6	0.5	Subsec-100	290	457	1351	2.6 – 160 (C – X5)
FSI	174[b]	314	9.0[f]	10-600	40.5	203	1985	7.4 (C1)
	304[b,e]				293	1089	10090	38.6 (C1)

a. HRI entrance aperture is 30 mm diameter.
b. Values are computed from CHIANTI spectra generated using the provided DEMs for CH, QS and AR. In the case of the C1 flare, the DEM from [1] was used.
c. For the 1216 Å channel, the detector is an essential part of the optical design avoiding additional filters to suppress the spectrum above 1300 Å. For this reason, the number of detected photons per px per second is given instead. The quantum efficiency is about 0.23 at 1216Å, 0.005 at 1600Å and 1.4×10^{-6} at 5000 Å.
d. Spectra from SUMER have been used to compute the count-rates in the 1216 Å channel in the case of QS and AR. CH values are obtained by scaling the QS value by the CH to QS ratio from [5]. Flare values are computed from the radiances of [3] for the C class and of [2] for the X5 class.
e. In the CHIANTI spectra the He II 304 Å radiances are forced to equal in CH and QS those from [5], in AR that from [4] and in the C1 flare that from [1].
f. The radiometric budget is estimated for a 9″ pixel, achieved by binning 2×2 the FSI images.

Table 5. : Channel capabilities and photon flux seen by the EUI.

90 HRI pixels or 22 EUS pixels, instead of 4 times these values with a 2k x 2k detector. The values promised by the 4k x 4k format are acceptable although one could hope for an even more gradual transition. Anyhow, the FSI optical design was shown to authorize this solution [7] and the corresponding telemetry increase can be handled by simple rebinning outside the region of interest or by more advanced lossy compression schemes [8]. Independently, the FSI telemetry allocation is felt as being underestimated.

As to the foreseen cadence, it has been an HRI design goal to make it in agreement to its spatial resolution. As shown in [9], time aliasing (whether undersampling or kinetic blurring) is to be avoided as much as possible.

5. CHALLENGES

Solar Orbiter is known to raise a number of technical issues, including to its payload [10]. Thermal matters come on top of the traditional aspects that affect EUV imaging telescopes: protection against contamination [11], ground- and space-based calibrations, mechanism reliability, baffling, alignments, etc. This will happen in a context where resources are sparse: mass, power and volume are restricted, while large baffles would be required to dilute the thermal load for example. In this section, we discuss two topics that are less often underlined, namely the availability of sufficient signal for given spatial and temporal resolutions and operational, telemetry, and software strategies. Needs for technological developments of EUI optical elements and the Heat Rejection Baffle are finally mentioned.

5.1. Radiometric considerations

Best estimates of the expected signal for all baselined channels and for various solar regions are reported in Table 5, which gives an overview of the channel sensitivity. For the EUV channels, the sensitivity is given as number of photons per second per pixel impinging on the detector. For the Lyman-α channel, the number of photons detected by the intensifier is provided.

Owing to its low (9.5") required angular resolution (still yielding a spatial resolution of about 1500 km at 0.22 AU) and to its high throughput, FSI enjoys a signal larger than 1000 detected $ph.px^{-1}.s^{-1}$ in Active Regions despite its small (5 mm) pupil diameter. Assuming Poisson noise dominance, FSI could run at 10 Hz while maintaining an SNR of 10 (in ARs). In contrast, and except for Lyman α observations, the high resolution payload is photon starving [9]. This is one of the main drivers in selecting coronal HRI bandpasses and the reason for their larger pupil diameter (30 mm minimum). The selected options offer nevertheless an SNR of at least 10 for a 4 s cadence (assuming uniform radiance within pixels and shot noise dominance). This will actually be a great breakthrough as such. Of course, the effective areas must still be improved as much as possible via optical elements progresses and instrumental design. We can also hope that the filling factor of some solar features will be low, enhancing the contrast of the scenes and the brightness of these objects. Finally, HRI observations of small flares will not encounter any shortage of photons. It is therefore meaningful to make the cameras able to run at a cadence of few Hz [9].

5.2. Operations, telemetry and onboard software

Another critical bottleneck of the EUI scientific aptitude resides in its telemetry (20 kbps), the suite being indeed capable of producing data in excess of the allocated rate by 2 to 3 orders of magnitude.

Maximizing the EUI science requires balanced strategies for target selection, *a posteriori* image filtering and data compression. Reference [8]

demonstrates compression of solar EUV images up to a factor 50 with only 0.01% of the pixels deviating more than the expected Poisson noise. Further progress of the compression ratio is being investigated. Yet, image compression alone cannot solve the telemetry shortage and onboard filtering of data based on predetermined science priorities and payload coordination is anticipated.

The EUI instrument suite does not have a pointing system for target selection but relies instead on the spacecraft pointing and tracking as a whole. Given the limited telemetry allocation, adequate target selection could be key in optimising the science output of EUI and the S.O. mission as a whole. Observation plans are intended to be uploaded a few weeks before the start of the perihelion passages.

However, most solar phenomena are sporadic and not predictable so that the most interesting events will likely be missed by predetermined plans. An autonomous payload mode could remedy this by determining on board the optimal pointing. While simple 'centre of disk' or pre-selected spacecraft pointing is undoubtedly the safest strategy for the first perihelion passage, it would be more rewarding to have target selection sometimes activated during later phases of the mission. Simple and robust algorithms can achieve this within the overall frame of preset operation programs. Such targets could include developing loop systems, newly emerged active regions, post-eruptive activity, dynamic filaments and Bright Points. These algorithms will be applied to FSI data and will output a preferred pointing target to the platform that can accept -or not- to switch the S/C and its payload into one among few preset modes.

Such an approach is studied by NASA [12] and also implemented by ESA for the PROBA2 satellite [13]. In combination with onboard notifications for *in situ* transient features, these algorithms can help to better link remote-sensing and *in situ* data.

5.3. Technological development of optical elements

Technological projects are ongoing to improve and/or assess the various critical elements of the EUI design. The development and testing of improved multilayers and metallic or interference filters is essential to the ultimate performance of the instrument as well as to its robustness against thermal stresses, ionizing particles, irradiation, dust or ageing. As to the focal plane imaging detectors, a number of options must be evaluated and compared. A project aiming at imaging devices based on wide bandgap semiconductors [14] is funded since the summer 2006. Back thinned APS and CCD are also among the options for the EUV channels, while intensified APS are the baseline for the HRI Ly α channel (Table 6). A back-thinned EUV sensitive low-noise CMOS-APS detector prototype is under development in Belgium and will serve for flight model development.

	Baseline	Back up	Augmented
HRI	2kx2k/10µm APS back-thin	2kx2k/10µm (CCD) 1kx1k/10µm (APS buttable) 1k x 1k APS/CCD	BOLD
FSI	4kx4k/10µm APS back-thin	2kx2k/10µm (APS buttable) 4kx4k/10µm (CCD) 2kx2k/20µm (APS/CCD)	BOLD

Table 6: Detector baseline, backup and augmented proposals of EUV detectors.

4.1.3 Feedthrough and baffles

The two HRI FOVs are 17 arcmin cones aligned with the optical axis, with at the vertex at 4122 mm and 6000 mm of the pupil centre for the HRI_{EUV} and $HRI_{Ly\alpha}$ respectively, and whose intersection with the pupil plane is a 30 mm diameter disc. The HRI clear aperture at the heat shield I/F is thus a 30 mm diameter disc located at the entrance section of the HRI entrance baffle. The FSI FOV is a 5.5 arcdeg square-based pyramid aligned with the optical axis, with the vertex at 53.05 mm of the pupil centre, whose intersection with the pupil plane is a 5x5 mm^2.

Each of the EUI units includes a front baffle, the aperture on the Sun side of these baffles being the optical pupil (*Figure 8* and *Figure 9*). In the HRIs and in the FSI, on the other end of these baffles are the EUV (or Lyman-α) entrance filters. It is not advisable to locate optical elements of the HRI on the heat shield itself, therefore our preferred option is to keep the HRI baffles on the instrument side, and use the heat shield opening as an additional protective baffle without optical diaphragm and without mechanical connection to the HRI units.

The HRI requires a conical aperture and the FSI a square-based pyramid aperture in the heat shield. The heat shield baffles are part of the spacecraft heat shield and must be outside the UFOVs of the instrument, plus a margin of 3-5mm (TBC depending on the expected thermo elastic behavior of the structure and the heat shield). This margin is a provision for misalignments and thermal movements between the heat shield and the EUI instrument entrance baffles. The heat load on the heat shield baffles is supposed to be dissipated by the heat shield itself. The heat shield baffles should not reflect any light inside the entrance pupils, to limit the

straylight and avoid an additional heat load. A way to achieve this could be to have structured heat shield baffles (grooves) or to implement edges in agreement with EUI team.

Anyway, there will be an infrared heat load from these baffles, due to their high temperature, with a substantial influence on the EUI thermal balance. In return, a part of the Sun light reflected by the HRI entrance baffles ends in the heat shield baffle, adding to its heat load.

The design of the HRI entrance baffles is based on a heat rejection mirror (HRM) placed at the level of the entrance filter, at a distance of 500 mm of the 30 mm ∅ entrance pupil, and on the specular reflectivity of the entrance filter. Considering the sun limb field of view (± 72.7 arcmin) to which is added a maximum off-pointing of 1.25 deg, the HRM diameter should be optimally 73 mm but the space between the HRM edge and the light beam going from the primary mirror to the secondary mirror is then too small. The HRM diameter has thus been reduced and a specific reflective baffle has been added to reject the heat load out of the baffle through the entrance pupil. This reflective baffle also rejects the light reflected by the filter foil. The HRM has a spherical shape with a radius of curvature of 700 mm, and a diameter of 61.7 mm. The baffle is composed of two connected elements: a reflective cylindrical tube in front of the HRM, and a reflective conical tube linking it to the entrance pupil.

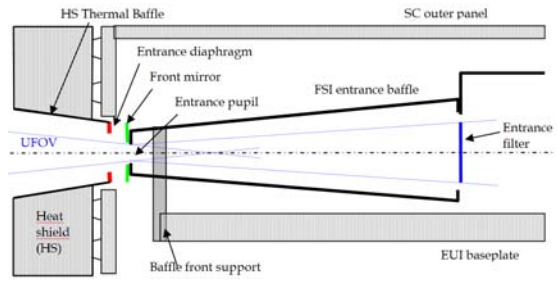

Figure 8 : FSI UFOV and heat shield interface.

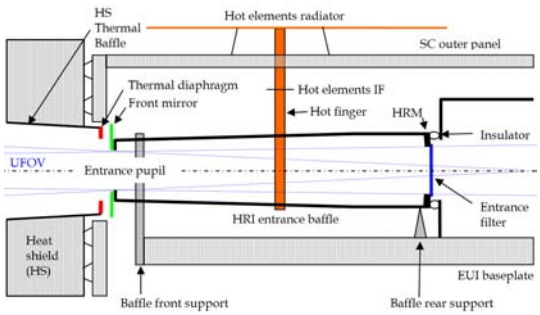

Figure 9: HRI UFOV and heat shield interface.

6. CONCLUSION

The EUI instrumental design and its science rationale have been presented. They illustrate the capabilities and the goals of a "general purpose" EUI suite, compliant with Solar Orbiter mission. The mission's ambitious characteristics draw severe constraints on the design of these instruments. The EUI instrument development plan which will require some trade-off between existing and promising technologies was presented and is feasible in the allocated time frame.

6. ACKNOWLEDGEMENT

The EUI instrument is developed in a collaboration which includes the Centre Spatial de Liège and Royal Observatory of Belgium (Belgium), the Institut d'Astrophysique and Institut d'Optique (France), the UCL Mullard Space Science Laboratory (UK), and Max Planck Institute for Solar System Research (Germany).

The Belgian institutions are funded by Belgian Federal Science Policy Office; the French institutions by Centre National d'Etudes Spatiales (CNES), the UK institution by Physics and Astronomy Research Council (PPARC); and the German institution by Deutsche Zentrum für Luft- und Raumfahrt e.V. (DLR).

6. REFERENCES

1. Andretta,V., Mauas, P., Falchi, A., Teriaca L., ApJ, Submitted
2. Lemaire, P., Gouttebroze, P., Vial, J.-C. et al., 2004, A&A 418, 737
3. Machado, M.E., Avrett, E.H., Vernazza, J.E., and Noyes, R.W., 1980, ApJ 242, 336
4. Mauas, P.J.D., Andretta, V., Falchi, A. et al., 2005, ApJ 619, 604
5. Vernazza, J.E. & Reeves, E.M., 1978, ApJSS 37,48
6. Teriaca L., Schühle U., Solanki S. K., Curdt W., Marsch E., *The lower transition region as seen in the H I Lyman-α line*, these Proceedings, SP-641, 2006
7. Auchere F.; Song X.; Rouesnel F.; Appourchaux T.; Fourmon J.-J; Le Clec'h J.-C.; Berthe M.; Defise J.-M.; Mazy E.; Rochus P. L.; Mercier R.; Ravet M.-F., *Innovative designs for the imaging suite on Solar Orbiter*, Solar Physics and Space Weather Instrumentation. Edited by Fineschi S.; Viereck R. A. Proceedings of the SPIE, Volume 5901, 298, 2005
8. Nicula B., Berghmans D., Hochedez J.-F., *Poisson recoding of solar images for enhanced compression*, Solar Physics, Volume 228, Issue 1-2, 253, 2005

9. Hochedez, J.-F.; Lemaire P.; Pace E.; Schühle U.; Verwichte E., *Wide bandgap EUV and VUV imagers for the Solar Orbiter*, In: Solar encounter. Proceedings of the 1st Solar Orbiter Workshop, 14-18 May 2001, Puerto de la Cruz, Tenerife, Spain, Eds.: B. Battrick & H. Sawaya-Lacoste, Scientific coordinators: E. Marsch, V. Martinez Pillet, B. Fleck & R. Marsden, ESA SP-493, 245, 2001
10. Fleck B.; Harrison R. A.; Marsden R. G.; Wimmer-Schweingruber R., *Summary of the Solar Orbiter payload working group activities*, Telescopes and Instrumentation for Solar Astrophysics. Edited by Fineschi, Silvano; Gummin, Mark A. Proceedings of the SPIE, Volume 5171, pp. 123-130, 2004
11. Schühle, U.; Thomas, R.; Hochedez, J.-F., *The Solar Orbiter Mission and Design Recommendations*, The Radiometric Calibration of SOHO, ISSI Scientific Report SR-002. Edited by A. Pauluhn, M.C.E. Huber and R. von Steiger. ESA Publications Division, Noordwijk, The Netherlands, p.361, 2002
12. Nelson, R. M.; Chmielewski, A.; Stevens, C. M.; Chien, S.; Davies, A.; Wyman, W., *NASA's New Millennium ST6 Project*, http://nmp.nasa.gov/st6/, American Geophysical Union, Spring Meeting 2005
13. Berghmans D., Hochedez J.-F., Defise J.-M., Lecat J.-H., Nicula B., Slemzin V., Lawrence G., Katsyiannis A. C., Van der Linden R. A. M., Zhukov A., Clette F., Rochus P., Mazy E., Thibert T., Nicolosi P., Pelizzo M-G. and Schühle U., *SWAP onboard PROBA 2, a new EUV imager for solar monitoring*, Advances in Space Research, Volume 38, Issue 8 , 1807-1811, 2006
14. Hochedez J.-F. E.; Schühle U. H.; Pau J. L.; Alvarez J.; Hainaut O.; Appourchaux T. P.; Auret F. D.; Belsky A.; Bergonzo P.; Castex M. C.; Deneuville A.; Dhez P.; Fleck B.; Haenen K.; Idir M.; Kleider J.-P.; Lefeuvre E.; Lemaire P.; Monroy E.; Muret P.; Munoz E.; Nesladek M.; Omnes F.; Pace E.; Peacock A. J.; Van Hoof C. A., *New UV detectors for solar observations*, Innovative Telescopes and Instrumentation for Solar Astrophysics. Edited by Stephen L. Keil, Sergey V. Avakyan . Proceedings of the SPIE, Volume 4853, 419-426, 2003